Geophysical Research Letters

RESEARCH LETTER
10.1029/2019GL082791

Thicker Clouds and Accelerated Arctic Sea Ice Decline: The Atmosphere-Sea Ice Interactions in Spring

Yiyi Huang[1], Xiquan Dong[1], David A. Bailey[2], Marika M. Holland[2], Baike Xi[1], Alice K. DuVivier[2], Jennifer E. Kay[3], Laura L. Landrum[2], and Yi Deng[4]

[1]Department of Hydrology and Atmospheric Sciences, University of Arizona, Tucson, AZ, USA, [2]Climate and Global Dynamics Laboratory, National Center for Atmospheric Research, Boulder, CO, USA, [3]Department of Atmospheric and Oceanic Sciences and Cooperative Institute for Research in Environmental Sciences (CIRES), University of Colorado Boulder, Boulder, CO, USA, [4]School of Earth and Atmospheric Science, Georgia Institute of Technology, Atlanta, GA, USA

Key Points:
- Active coupling is found between the atmosphere and sea ice in early spring
- Clouds are one of important drivers for sea ice melting from April to June

Supporting Information:
- Supporting Information S1

Correspondence to:
X. Dong,
xdong@email.arizona.edu

Citation:
Huang, Y., Dong, X., Bailey, D. A., Holland, M. M., Xi, B., DuVivier, A. K., et al. (2019). Thicker clouds and accelerated Arctic Sea ice decline: The atmosphere-sea ice interactions in spring. *Geophysical Research Letters*, *46*, 6980–6989. https://doi.org/10.1029/2019GL082791

Received 12 MAR 2019
Accepted 20 MAY 2019
Accepted article online 28 MAY 2019
Published online 19 JUN 2019

Abstract Observations show that increased Arctic cloud cover in the spring is linked with sea ice decline. As the atmosphere and sea ice can influence each other, which one plays the leading role in spring remains unclear. Here we demonstrate, through observational data diagnosis and numerical modeling, that there is active coupling between the atmosphere and sea ice in early spring. Sea ice melting and thus the presence of more open water lead to stronger evaporation and promote cloud formation that increases downward longwave flux, leading to even more ice melt. Spring clouds are a driving force in the disappearance of sea ice and displacing the mechanism of atmosphere-sea ice coupling from April to June. These results suggest the need to accurately model interactions of Arctic clouds and radiation in Earth System Models in order to improve projections of the future of the Arctic.

Plain Language Summary Arctic summer sea ice has declined by nearly 50%, leading to a larger exposed area of open water that persists longer than before. Clouds have large influences on Arctic sea ice long-term trends and variability. Atmosphere and sea ice are believed to actively interact with each other in spring. But attributing cause and effect is difficult. Therefore, this study seeks to answer the following question: does the atmosphere primarily drive the sea ice changes or does the sea ice dominate changes in the atmosphere in spring? In this study, we isolated the atmospheric response to Arctic sea ice changes from coupled system through both observations and model simulations. It suggests that this relationship is initiated with active coupling in March. Spring clouds then become a driving force in the disappearance of sea ice from April to June. Overall, identifying the two-way interactions between Arctic sea ice and atmosphere is a critical step to improve seasonal sea ice forecasts and future sea ice prediction. The sea ice coverage and length of the open water season is important for human activities and wildlife. The long-term time series will inform future planning of military, civilian, and commercial infrastructure.

1. Introduction

The Arctic near-surface and lower troposphere are warming faster than the globe as whole, which is known as Arctic amplification (e.g., Holland & Bitz, 2003). Surface-based arctic amplification is largely driven by sea ice loss, which allows for enhanced shortwave absorption at the surface and energy transfer to from the ocean to the atmosphere with a seasonal delay (e.g., Boisvert & Stroeve, 2015; Serreze et al., 2009). Over the last few decades, thinner, less expansive Arctic sea ice and a longer melting season have been observed (Markus et al., 2009; Notz & Stroeve, 2018; Serreze & Stroeve, 2015). Since the dawn of the satellite era, Arctic summer sea ice has declined by nearly 50% and has accelerated in the early twenty-first century (Comiso et al., 2008; Notz & Stroeve, 2018; Serreze & Stroeve, 2015), leading to a larger exposed area of open water that persists longer than before.

Both dynamic and thermodynamic forces drive sea ice decline. Among them, clouds have a large influence on Arctic radiation budgets and thus can impact Arctic sea ice long-term trends and variability. Previous studies using surface and satellite observations as well as reanalysis products have concluded that the enhanced longwave forcing due to increased cloudiness and water vapor can accelerate sea ice melt in early spring, while cloud impacts on absorbed solar radiation become more important for surface warming and sea ice melt in early summer (e.g.,Cox et al., 2016; Kapsch et al., 2013). The observed sea ice change is

also altering the exchange of mass, energy, and momentum between the Arctic Ocean and atmosphere. For example, Atmospheric Infrared Sounder results reveal that the rate of evaporation and moisture flux have increased over the Arctic regions between 2003 and 2013, a development mainly driven by sea ice loss and increases in skin temperature (Boisvert et al., 2015; Boisvert & Stroeve, 2015). Spaceborne lidar observations show that more low-level clouds are found over newly open water during autumn, spring, and winter, while summer is the only season without change (Kay & Gettelman, 2009; Morrison et al., 2018). These changes in cloud coverage and other properties can alter surface radiative fluxes and further affect sea ice melt and growth. While seasonal differences in observed cloud-sea ice relationships are consistent with the air-sea coupling hypothesis (Kay & Gettelman, 2009; Morrison et al., 2018), attributing cause and effect is always difficult in a coupled system. In general, atmosphere and the sea ice are believed to actively interact with each other in spring, as suggested by observations (e.g., Kay & Gettelman, 2009). Therefore, this study seeks to answer the following questions with greater precision: does the atmosphere primarily drive the sea ice changes or does the sea ice dominate changes in atmosphere in the spring, and how do these relationships differ by month? A better understanding of cloud-radiation-sea ice interactions is essential to represent this relationship in fully coupled Earth System Models and further improve forecasts of sea ice on seasonal and longer time scales.

Since clouds and their radiative impacts are known to be critical to Arctic climate feedback (e.g., Dong et al., 2010; Kay et al., 2012), we will particularly examine cloud properties such as cloud fraction (CF) and cloud water path (CWP), as well as related radiative flux changes at the surface. CF is the percentage of each pixel in satellite imagery or each grid box in a climate model that is covered with clouds. CWP is defined as the sum of cloud liquid water path (LWP) and ice water path (IWP). Specifically, LWP is the measure of the weight of liquid water droplets in the atmosphere above a unit surface area on the Earth, while IWP is defined as the integral of the ice water content through the depth of an ice cloud layer (Heymsfield et al., 2003). Both CF and CWP play a major part in the Arctic's energy budget (Curry et al., 1996). In general, downward longwave radiative flux (LW_down) at the surface mostly depends on CF instead of CWP as the Arctic clouds are generally optically thick. Within the clouds, liquid water substantially increases the cloud longwave effect compared to ice water (Shupe & Intrieri, 2004). CWP has a large impact on shortwave flux as thick clouds reflect sunlight back into space, which causes cooling (Curry et al., 1996). The changes in radiative balance above the sea ice are important for its melt and growth.

Through an integrative analysis of observation and modeling, we have isolated the atmospheric response to Arctic sea ice changes from the atmosphere-sea ice coupled system. We focus on the transitional springtime months from March to June both because observational studies have determined large signals during this time and it is a period important for sea ice seasonal forecasts (Cox et al., 2016; Huang, Dong, Xi, Dolinar, & Stanfield, 2017; Kapsch et al., 2013). To disentangle the role of coupled interactions, we compare coupled CESM-Large Ensemble (CESM-LE) experiments (Kay et al., 2015) with atmosphere-only experiments that use prescribed sea ice conditions. Overall, identifying the two-way interactions between sea ice cover and Arctic cloud/radiation properties is a critical step to increase the precision of seasonal sea ice forecasts and to predict the rate of future sea ice loss.

2. Data, Model, and Methods

Cloud properties including CF and CWP used in this study are from the Clouds and Earth's Radiant Energy System (CERES)–Moderate Resolution Imaging Spectroradiometer (MODIS) SYN1 Edition 3A monthly gridded data set (1° × 1°) (Minnis, Sun-Mack, Young, et al., 2011; Minnis, Sun-Mack, Chen, et al., 2011; Wielicki et al., 1996). In the Arctic, annual mean CFs from CERES-MODIS observations have a negative bias of −11.2% compared to active remote sensor Cloud-Aerosol Lidar and Infrared Pathfinder Satellite Observation (CALIPSO; Huang, Dong, Xi, Dolinar, Stanfield, & Qiu, 2017). The surface radiation fluxes are from CERES Energy Balanced And Filled (EBAF)-Surface Edition 2.8 data sets. Details about uncertainties of global surface radiative fluxes can be found in Kato et al. (2013) and CERES-EBAF data quality summary (2015). Moreover, Huang, Dong, Xi, Dolinar, Stanfield, and Qiu (2017) clearly quantified their uncertainties over the Arctic. Previous studies concluded that CERES-EBAF surface should be considered as a key benchmark for evaluating the Arctic surface radiation budget (Boeke & Taylor, 2016; Christensen et al., 2016). Sea ice observation is obtained from Nimbus-7 SSMR and DMSP SSM/I-SSMIS passive microwave data version 1 provided by the National Snow and Ice Data Center (Cavalieri et al., 1996). The

uncertainty of sea ice concentration over the Arctic is within ±5% during the winter and increases to ±15% during the summer with presence of melt ponds over sea ice (Cavalieri et al., 1992).

To further examine whether the Earth System Model is capable to capture the observed features, we mainly focus on model simulations from CESM-LE project, which provides a comprehensive resource for studying climate change in the presence of internal climate variability (Kay et al., 2015). The CESM-LE is run with fully coupled atmosphere, ocean, land, and sea ice components from 1920 to 2100. For this study we use the monthly mean atmospheric variables from 40 members of the CESM-LE, which is provided in a grid of 0.94°(latitude) × 1.25°(longitude; Kay et al., 2012, 2015). Overall, CESM can capture general Arctic cloud, radiation, and sea ice features (Barton et al., 2012; Kay et al., 2012; Hurrell et al., 2013). And their biases have been clearly quantified using observations in previous studies (e.g., Barton et al., 2012). Particularly, Community Atmosphere Model version 5 simulated Arctic CF is biased about twice as much winter cloud as the CALIPSO observations. When compared appropriately using a cloud simulator, the seasonal cycle of simulated CF is in better agreement with observed one (Kay et al., 2012, 2016). Moreover, Community Atmosphere Model version 5 has too few liquid clouds in the Arctic. Therefore, it is not surprising that CESM-LE underestimates LW_down flux at the surface (McIlhattan et al., 2017). Despite the mean state being biased in the model, CESM reproduces the present-day observed cloud response to sea ice variability (Morrison et al., 2019). We do understand that Arctic cloud and radiation properties are not perfectly simulated by CESM; however, it is still an important tool for us to understand causal relationship in Arctic climate system.

In addition to analyzing observations and CESM-LE output, a CESM atmosphere-only experiment was conducted to investigate the uncoupled atmospheric response to forcing from different September sea ice extent trends. Due to internal climate variability, all 40 members in CESM-LE exhibit different linear trends in the Northern Hemisphere in early twenty-first century (2006–2021). Seven ensemble members (members 15, 40, 12, 30, 17, 25, 13) among them are selected (Figure S1 in the supporting information) to provide a large contrast in September sea ice extent linear trends. We then calculate the regression slope between September sea ice extent and sea ice thickness in each grid cell for 12 months over the Arctic (Figure S2 in the supporting information) using all 40 members from CESM-LE. The same methods are also applied for sea ice concentration and sea surface temperature (not shown). Based on the monthly regression maps between September sea ice extent and sea ice-related variables, we then generate the sea ice input data files for seven selected members separately to use as prescribed surface conditions for the Atmospheric Model Intercomparison Project (AMIP)-style simulations. Specifically, different values in the sea ice-covered regions are used in the Northern Hemisphere and 40-member ensemble mean in the tropics and Southern Hemisphere. Seven CESM AMIP experiments are then run with active atmosphere and land models and the different prescribed sea ice concentration, sea surface temperature, and sea ice thickness. We use external forcing Representative Concentration Pathway 8.5 (RCP8.5) from 2006 to 2021 and same spatial resolution as CESM-LE.

Due to the different spatial resolutions of the satellite products, sea ice concentration data are regridded from their native 25 km × 25 km to 1° × 1° resolution to make them comparable to the CERES-MODIS SYN1 and CERES EBAF data sets. Note that 16-year linear trends and correlations are calculated when there are more than eight years of data for both satellite products and CESM-LE. We avoid using all available time steps in the raw data for statistical significance test. Instead, following the method in Bretherton et al. (1999), we use effective sample size by considering the impact of secular trend on the correlation. The evaporation rate in Figure 3 is converted from latent heat flux at 0 °C from CESM model output, which is, the unit evaporation rate is roughly equal to 28.94 W/m^2 of upward latent heat flux.

3. Results

3.1. Trends of Arctic Clouds in Early Twenty-First Century

Figure 1 shows the linear trends of total CF over the Arctic during spring (March–June) 2000–2015 from observations. As shown in Figures 1a–1d, there are significant positive CF linear trends in spring from NASA CERES-MODIS satellite retrievals, especially from March to May (Figures 1a–1c). Specifically, relatively large increasing trends are found over the Siberian Sea, Laptev Sea, and Kara Sea in March and April. At the same time, September sea ice concentration has been retreating rapidly over these regions during the period of 2000–2015 (Figure 1e). A previous study found that there are significant negative correlations between springtime CF and September sea ice concentration in the early twenty-first century (Huang,

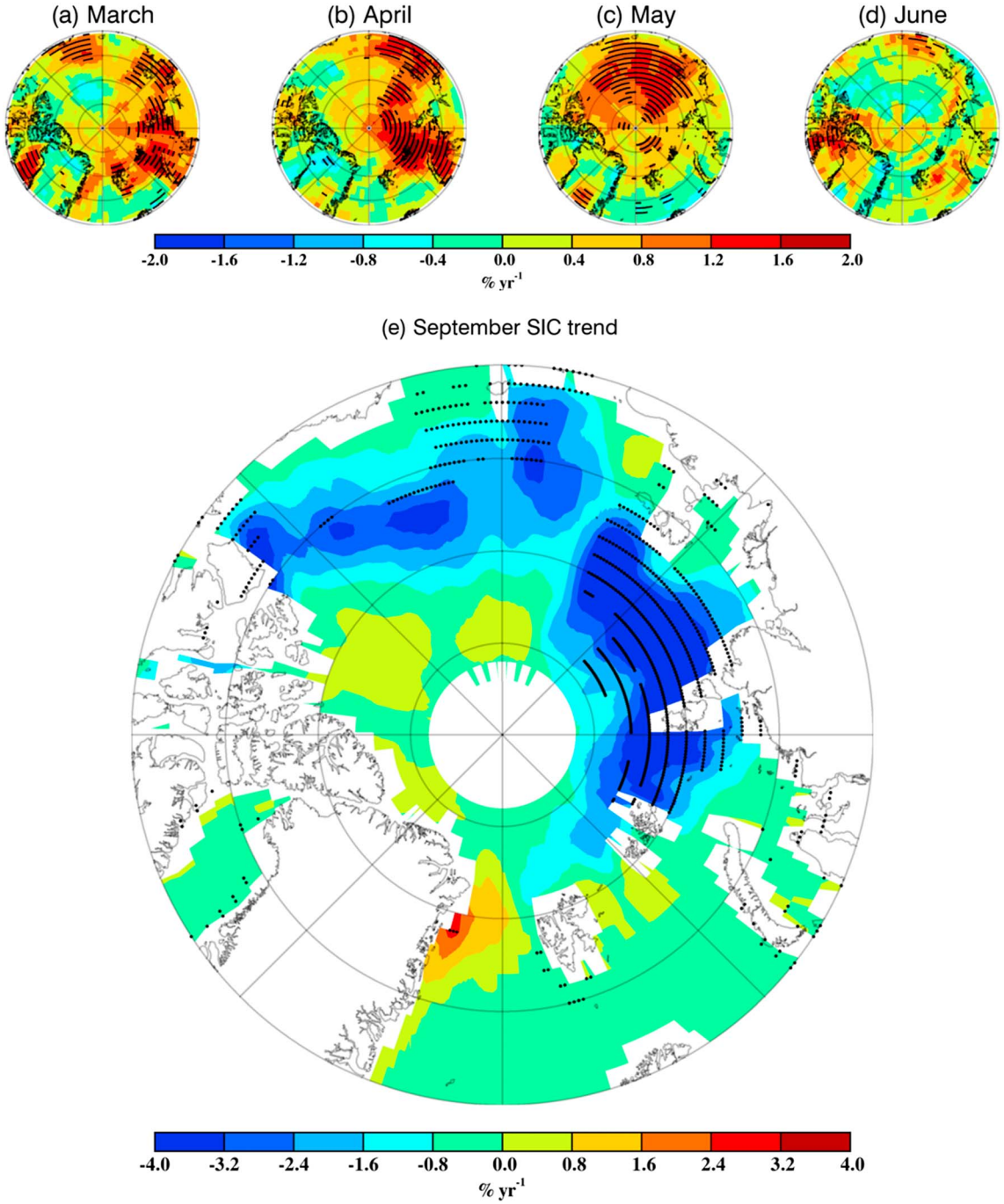

Figure 1. The linear trends of satellite retrieved (a–d) cloud fractions from March to June and (e) September sea ice concentration (SIC) over the Arctic (70°–90°N) regions in early twenty-first century (2000–2015). Cloud observations are derived from CERES-MODIS SYN1 Ed3.0 product. The black dots mark the regions where $p < 0.05$ (statistical significance at 95% confidence level). Note that Figure 1e was obtained and modified from Figure 1 in Huang, Dong, Xi, Dolinar, and Stanfield (2017).

Dong, Xi, Dolinar, & Stanfield, 2017), indicating a potential predictability for autumn Arctic sea ice extent with cloud observations in early spring.

Earth System Models are important tools for understanding mechanisms driving Arctic change. Therefore, we examine 40 members from the fully coupled model CESM to evaluate whether they capture linear trends in CF that are comparable to observations. In fact, the simulated CF linear trends differ considerably across the 40 members in the CESM-LE (Figure S3 in the supporting information). Since all 40 ensemble members

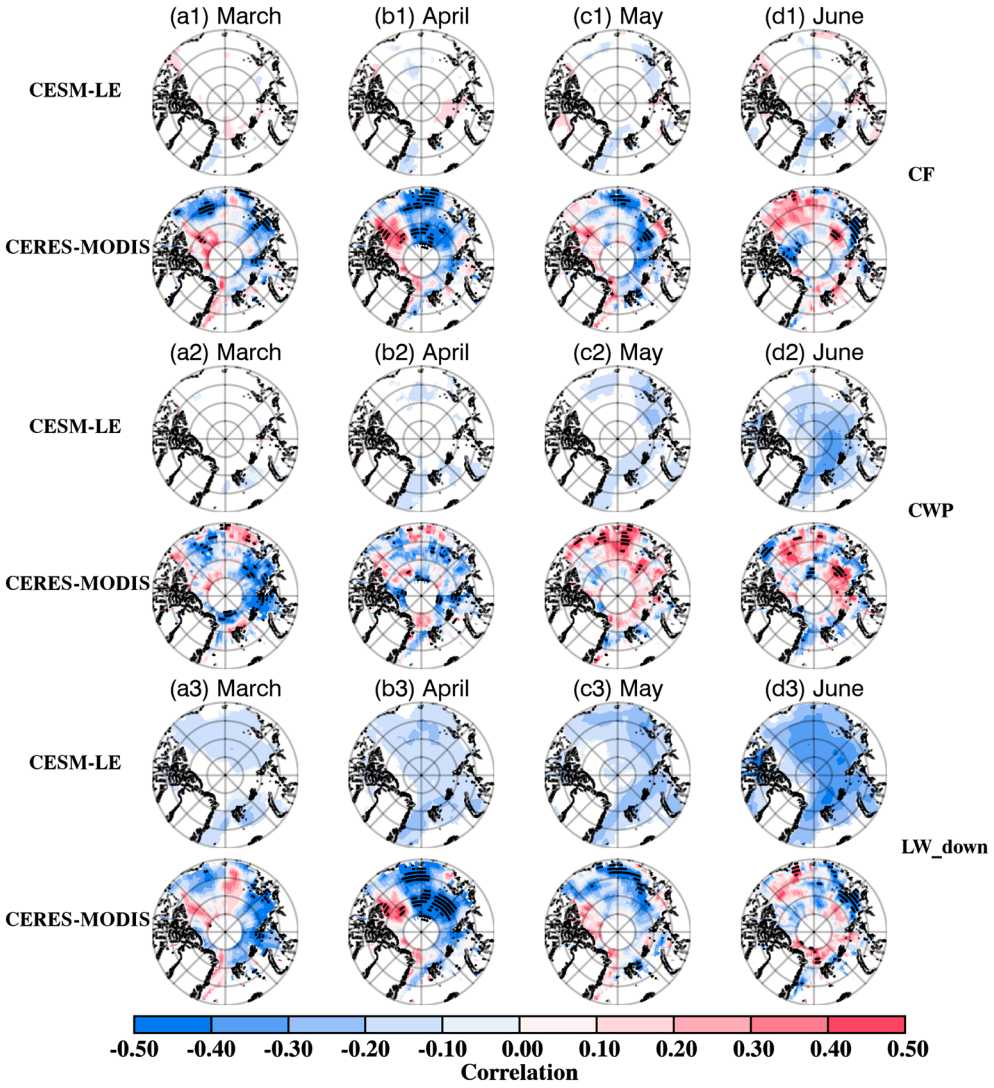

Figure 2. The correlations between (a1–d1) springtime total CF and September sea ice concentration (SIC) in CESM-Large Ensemble (CESM-LE; upper, 2006–2021) and CERES-MODIS (lower; 2000–2015), (a2–d2) springtime total cloud water path (CWP) and September SIC in CESM-LE (upper) and CERES-MODIS (lower), and (a3–d3) springtime downward longwave (LW_down) flux at the surface and September SIC in CESM-LE (upper) and CERES-MODIS (lower) from March to June in the early twenty-first century. The black dots mark the regions where $p < 0.05$ (statistical significance at 95% confidence level) for CERES-MODIS. Note that only the correlations with 95% statistically significance level are shown in CESM-LE due to large number of data points (640 data samples).

use the same model and same external forcing with only small round-off level differences in their atmospheric initial conditions in 1920, their spread in CF linear trends can be attributed to internally generated climate variability alone (Kay et al., 2015). The comparison between satellite retrievals and each ensemble member in CESM-LE suggests that the observed positive linear trends of Arctic CF in the early twenty-first century are likely due to internal climate variability. But the observed increasing CF trends in early spring still have found to enhance sea ice melt and further affect sea ice trends (e.g., Huang, Dong, Xi, Dolinar, & Stanfield, 2017), so understanding the relationship between clouds and sea ice is important.

3.2. Relationships Between September Sea Ice Minimum With Springtime Cloud and Radiation Properties

To better reveal the relationships between September sea ice and springtime cloud and radiation properties, the correlations between these variables are shown in Figure 2. Note that the black dots mark the regions where correlations are 95% statistically significant for CERES-MODIS, but only the correlations with 95%

statistically significance level are shown in CESM-LE due to large sample size. From observational perspective, negative correlations between springtime CF and September sea ice concentration are found from March to May with the strongest negative correlations in April (Figures 2a1–2d1). As a primary cause of the cloud warming effects, increasing surface LW_down flux tends to reduce September sea ice concentration by warming the surface at the same time as CF, as demonstrated in Figures 2a3–2d3. Although LW_down flux at the surface is not necessarily caused by clouds, previous studies have demonstrated the important contributions of surface warming from clouds to the sea ice melting in spring (Dong et al., 2014; Huang, Dong, Xi, Dolinar, & Stanfield, 2017; Huang et al., 2018). In springtime, the averaged LWP over the entire Arctic is greater than the saturation value (30 g/m^2) and after this point clouds emit as blackbodies, so that LW_down flux mostly depends on CF (Shupe & Intrieri, 2004). The negative correlations between September sea ice concentration and CWP in March and April suggest that the cloud longwave effect results in clouds warming the surface, and further enhancing sea ice melt. While more widespread positive correlations in May and June (Figures 2c2 and 2d2) suggest that the influence of CWP on shortwave flux dominates at this time, resulting in clouds cooling the surface. Previous studies have demonstrated the importance of cloud shortwave effect on Arctic sea ice melting in early summer based on both surface and satellite observations (Choi et al., 2014; Cox et al., 2016; Dong et al., 2014; Huang, Dong, Xi, Dolinar, & Stanfield, 2017).

In contrast to observations, through the four months the CESM-LE indicates a relatively weak linkage between springtime CF and September sea ice concentration, while the relationship between CWP and September sea ice concentration are much stronger, especially from April to June (Figures 2a2–2d2). In particular, these relationships are strongest over the Atlantic sector of Arctic Ocean where the relatively large sea ice melting occurs in early spring (not shown). Furthermore, the negative correlations are found in LW_down flux at the surface, suggesting that the cloud longwave effect on the sea ice melting increases from March to June in CESM-LE on a seasonal basis (Figures 2a3–2d3). But the cloud shortwave effect in early summer cannot be well captured from CWP perspective. Note that there are large differences in the number of samples used for the correlation analysis for the CESM-LE ($N = 640$) and the satellite retrievals ($N = 16$), which may affect the spatial distribution and magnitude. More appropriately, if instead we compare analysis from each individual member with observations, different members exhibit various spatial patterns due to internal variability. But their magnitudes of correlations are much closer to observed ones (Figure S6 in the supporting information). In CESM-LE, the correlation patterns in surface LW_down flux match better with CWP than CF. This can be explained by insufficient simulated LWP across the Arctic in the CESM (Kay et al., 2016). Since the simulated LWP values are much less than 30 g/m^2 over the Arctic in spring, longwave cloud forcing would substantially increase with LWP (Shupe & Intrieri, 2004). As September sea ice changes are largely controlled by LW_down flux at the surface, sea ice changes in CESM are more likely to be affected by CWP rather than CF.

To better explain interannual variability and reduce the effects of long-term trend, we remove the trend in the raw data and recalculate their correlations (Figure S7 in the supporting information) to compare with nondetrended results (Figure 2). From observational perspective, the negative correlations in CF and surface LW_down flux over the Laptev/Siberian Sea become much weaker after detrending the data. This is consistent with the conclusion from previous study (Huang, Dong, Xi, Dolinar, & Stanfield, 2017): that is, the Laptev/Siberian Sea shows most significant long-term trends of cloud/radiation properties in spring, while it is more meaningful to relate the impact of springtime cloud/radiation properties on September sea ice retreat at interannual time scale over the Chukchi/Beaufort Sea. But there is no substantial difference between detrended and nondetrended results in CESM-LE.

Although there are small differences, both CESM-LE and CERES-MODIS observations demonstrate a similar relationship where increases in springtime clouds and associated radiation effects are related to decreased sea ice in September. However, the causality in this relationship cannot be clearly identified either using observations or CESM-LE simulations as both are in an atmosphere-sea ice coupled environment. Therefore, a CESM atmosphere-only experiment was conducted to examine the uncoupled atmospheric response to forcing from different September Arctic sea ice extent trends.

3.3. The Atmospheric Response Under Different Arctic Sea Ice Trends

Figure 3 shows the linear trends of cloud and radiation properties for March in the AMIP experiments under different prescribed September sea ice extent trends during the period 2006–2021. These members are

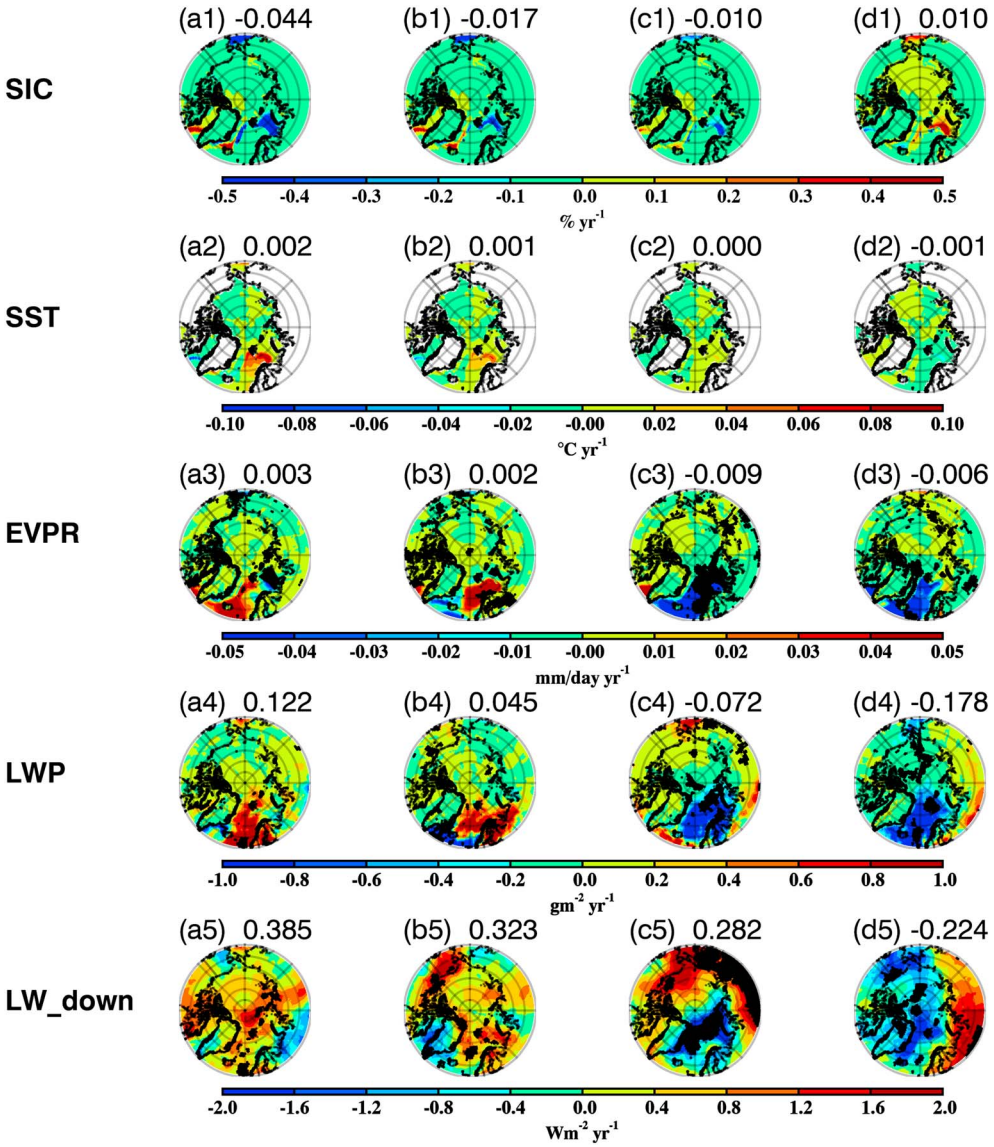

Figure 3. The linear trends of Arctic (a1–d1) sea ice concentration (SIC), (a2–d2) sea surface temperature (SST), (a3–d3) evaporation rate (EVPR), (a4–d4) liquid water path (LWP), and (a5–d5) downward longwave flux (LW_down) at the surface for March in the early twenty-first century (2006–2021) in CESM AMIP experiments. The four selected members (members 15, 12, 17, 13) are displayed from the most negative sea ice extent (SIE) trend (left) to most positive SIE trend (right) in September. The numbers of linear trends over the Arctic (60°N northward) are shown at the top of each panel. The black dots mark the regions where $p < 0.05$ (statistical significance at 95% confidence level). Note that SIC and SST are prescribed in the CESM AMIP experiment, so their linear trends are statistically significant everywhere.

displayed in Figures 3a1–3d1 from the most negative sea ice trend (left) to the most positive trend (right). The largest trends in sea ice reduction (increase) are found in the Atlantic sector of the Arctic Ocean and Bering Sea. With more sea ice loss and increased sea surface temperature, relatively stronger evaporation is observed in the region (Figures 3a3–3d3). As a result, an increasing trend of LWP is enhanced (Figures 3a4–3d4) with faster sea ice decline and surface warming. Meanwhile, an increase in sea ice extent (Figure 3d1) and sea surface cooling (Figure 3d2) are related to reduced LWP (Figure 3d4). The LWP results are highlighted here because the presence of liquid water substantially increases the cloud longwave effect compared to ice water (Shupe & Intrieri, 2004). From Figures 3a5–3d5, the increasing trends of LW_down flux at the surface tend to increase with larger sea ice retreat, higher temperature, stronger evaporation, and increased cloud water. Although other factors, such as coupling with lower

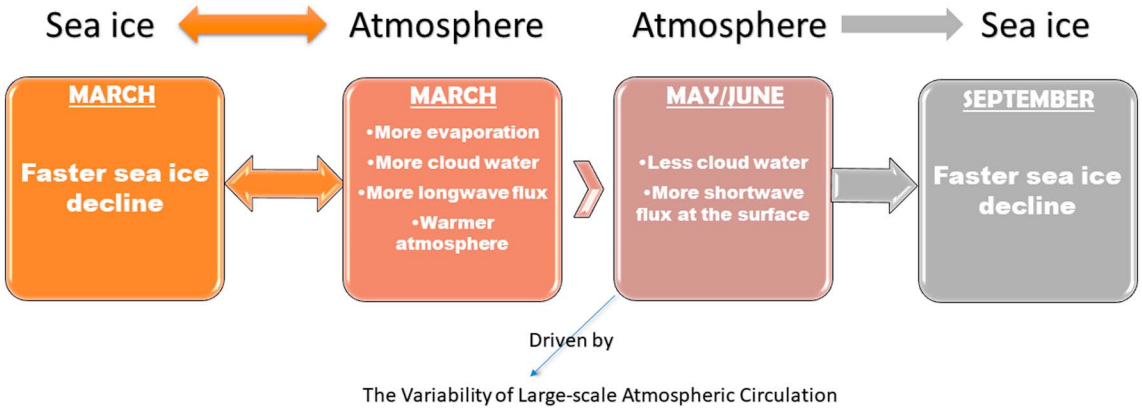

Figure 4. Schematic diagram describing interactions between springtime cloud and radiation properties and Arctic September sea ice decline.

latitudes, will modify the exact trends simulated across our AMIP members, these qualitative relationships between the rate of sea ice retreat and changing atmospheric conditions are generally valid for all seven members (Figure S8 in the supporting information).

In particular, a clear atmosphere response (CWP, evaporation rate, and surface LW_down flux) to different sea ice extent trends only can be found in March as changes in key atmospheric variables are highly affected by sea ice decline/increase (Figure S9 in the supporting information). The trends of related atmospheric variables in the other three months are random, indicating that there are no significant atmosphere responses with different sea ice retreat rates in late spring. The cloud response to sea ice loss largely depends on the strength of atmosphere–ocean coupling which is modulated by air-sea temperature gradients and near-surface static stability in the Arctic (Kay & Gettelman, 2009). Specifically, CF and LWP increase with decreased atmospheric stability as shown by the NASA A-Train active remote sensing data (Taylor et al., 2015). In early spring, when the ocean surface is covered by sea ice, the static stability is relatively low as the air-sea temperature gradient is strong; therefore, clouds are normally formed over newly opened water because of turbulent transfer of heat and moisture flux. More specifically, Arctic low clouds are more easily formed in an unstable environment when cool air overlies a relatively warm surface. In this case, there is strong surface-atmosphere coupling through upward moisture and heat fluxes due to an unstable boundary layer, as shown in Figures 3a3–3d3. This cloud formation process is usually found in the North Atlantic (Kay & Gettelman, 2009). In contrast, when there is a weaker air-sea temperature gradient as occurs with a melting sea ice surface, a more stable atmosphere limits the turbulent flux exchange leading to a reduced effect on cloud formation (Herman & Goody, 1976; Kay & Gettelman, 2009; Taylor et al., 2015).

The comparison between coupled CESM-LE simulations and forced AMIP experiments helps to disentangle the roles of springtime clouds and radiation in affecting sea ice trends. The CWP linear trends in these seven CESM AMIP members and CESM-LE are different from each other for all four months at 95% significance level (Figure S10 in the supporting information). By comparing the relationships from the CESM-LE and AMIP experiments, it is evident that the atmosphere and sea ice have a two-way interaction in March. With accelerated sea ice retreat and surface warming, the presence of open water can enhance evaporation, which favors the formation of clouds, and therefore reinforces surface warming through downward longwave flux changes that further enhance sea ice melting. But starting from April, atmosphere has little response to the changes in sea ice either from long-term trend or year-to-year climate variability (not shown). The significant observed positive linear trends of CFs in April and May in the early twenty-first century (Figure 1) exhibit strong negative correlations with September sea ice retreat (Figure 2) from satellite retrievals. These cloud changes mainly result from large-scale atmospheric circulation variability (Ding et al., 2017; Huang et al., 2018; Kay & Gettelman, 2009). More precisely, previous studies found that a stronger anticyclonic circulation over Arctic Ocean with a barotropic structure in the troposphere is an important contributor to low-level warming during the period 1979–2014. This near-surface warming was caused by increasing LW_down flux above the sea ice which resulted from increased low clouds and water vapor (Ding et al., 2017).

4. Summary and Discussion

The schematic diagram for Arctic cloud-radiation-sea ice interactions are shown in Figure 4. The conclusions drawn in this study are based on the evidence from both observations and model simulations. The increasing trend of Arctic clouds in spring is found to be highly correlated with sea ice retreat in the early twenty-first century. The cloud longwave effect results in warming the surface in early spring, while cloud shortwave effect dominates in late spring and early summer. Although cloud shortwave effect on sea ice is not well captured by CESM, satellite observations have demonstrated that amount of absorbed solar radiation in early summer, which is largely controlled by clouds, exhibits significant negative correlations with Arctic sea ice concentration in late summer (Choi et al., 2014). Moreover, Huang, Dong, Xi, Dolinar, and Stanfield (2017) suggested that increasing surface downward shortwave flux in late spring should be attributed to decreasing CWP in the early twenty-first century from observational perspective.

In general, the fully coupled model CESM has difficulties in reproducing this observed cloud-radiation-sea ice relationship. A deeper understanding of cause and effect between these variables would help fill in this gap. Comparing CESM AMIP experiments with different prescribed ice loss rates, we can isolate the atmospheric response to changes in Arctic sea ice from those associated with atmosphere-sea ice coupling. In early spring, the atmosphere and sea ice are strongly coupled (two-way interactions). From April to June, however, the impacts of cloud and radiation on sea ice become dominant and sea ice has a limited influence on the overlying atmosphere. The changes in cloud during this period are instead mainly controlled by large-scale atmospheric circulation variability.

As sea ice cover is expected to continue shrinking under the projected RCP8.5 scenario, we also examine the future relationships between cloud, radiation, and sea ice in early, middle, and late twenty-first century through CESM-LE. The most prominent shift of surface LW_down flux linear trends occurs in March and April (Figure S12 in the supporting information), during which the correlations between LW_down flux and sea ice become more negative in the late twenty-first century (Figure S13 in the supporting information). Therefore, the impacts of cloud and radiation properties on sea ice melting tend to shift to early spring and become stronger in the middle and late twenty-first century.

These results improve our understanding of cloud process and its influence on surface energy budget as well sea ice melt over the Arctic. This will inform the Earth System Models with a more realistic cloud-radiation process that governs the seasonal sea ice evolution. In addition, with a better representation of observed cloud-radiation-sea ice relationship, we can substantially improve Earth System Models' ability in simulating and predicting future Arctic sea ice changes.

Acknowledgments
This work was supported by the NASA Earth and Space Science Fellowship program to Y. Huang at the University of Arizona (80NSSC18K1339), under the advisement of Xiquan Dong. X. Dong and B. Xi were supported by NASA CERES project through grant 80NSSC19K0172 at the University of Arizona. This material was also based upon work supported by the National Center for Atmospheric Research (NCAR), which is a major facility sponsored by the National Science Foundation (NSF) under cooperative agreement 1852977. J. E. Kay was supported by NASA under grant 15-CCST15-0025. Y. Deng was supported by the NSF under grants AGS-1354402 and AGS-1445956 and by National Oceanic and Atmospheric Administration under award NA16NWS4680013. We would like to thank NCAR Advanced Study Program Graduate Visitor Program, as well as acknowledge high-performance computing support from Cheyenne (doi:10.5065/D6RX99HX) provided by NCAR's Computational and Information Systems Laboratory, sponsored by the National Science Foundation. In addition, we appreciate Christopher Cokinos for proofreading as well as two anonymous reviewers for their constructive comments and suggestions. In this study, sea ice concentrations from Nimbus-7 SMMR and DMSP SSM/I-SSMIS Passive Microwave Data, version 1 are accessed from NASA DAAC at the National Snow and Ice Data Center at http://nsidc.org/data/docs/daac/nsidc0051_gsfc_seaice.gd.html#cavalieri_92. While NASA CERES SYN1deg and CERES-EBAF surface data sets are available at http://ceres.larc.nasa.gov/order_data.php. The output of CESM-Large Ensemble project is available on NCAR High Performance Storage System (HPSS) on Cheyenne (http://www.cesm.ucar.edu/projects/community-projects/LENS/data-sets.html). CESM AMIP experiment output is available from corresponding author upon request.

References

Barton, N. P., Klein, S. A., Boyle, J. S., & Zhang, Y. Y. (2012). Arctic synoptic regimes: Comparing domain-wide Arctic cloud observations with CAM4 and CAM5 during similar dynamics. *Journal of Geophysical Research*, *117*, D15205. https://doi.org/10.1029/2012JD017589

Boeke, R. C., & Taylor, P. C. (2016). Evaluation of the Arctic surface radiation budget in CMIP5 models. *Journal of Geophysical Research: Atmospheres*, *121*, 8525–8548. https://doi.org/10.1002/2016JD025099

Boisvert, L. N., & Stroeve, J. C. (2015). The Arctic is becoming warmer and wetter as revealed by the Atmospheric Infrared Sounder. *Geophysical Research Letters*, *42*, 4439–4446. https://doi.org/10.1002/2015GL063775

Boisvert, L. N., Wu, D. L., & Shie, C. L. (2015). Increasing evaporation amounts seen in the Arctic between 2003 and 2013 from AIRS data. *Journal of Geophysical Research: Atmospheres*, *120*, 6865–6881. https://doi.org/10.1002/2015JD023258

Bretherton, C. S., Widmann, M., Dymnikov, V. P., Wallace, J. M., & Bladé, I. (1999). The effective number of spatial degrees of freedom of a time-varying field. *Journal of Climate*, *12*(7), 1990–2009. https://doi.org/10.1175/1520-0442(1999)012<1990:TENOSD>2.0.CO;2

Cavalieri, D. J., Crawford, J., Drinkwater, M., Emery, W. J., Eppler, D. T., Farmer, L. D., et al. (1992). NASA Sea Ice Validation Program for the DMSP SSM/I: Final Report, NASA Technical Memorandum 104559 (126 pp.). National Aeronautics and Space Administration, Washington, DC.

Cavalieri, D.J., Parkinson, C., Gloersen, P., & Zwall, H. J. (1996). Sea ice concentrations from Nimbus-7 SMMR and DMSP SSM/I-SSMIS Passive Microwave Data, version 1. Boulder, CO: NASA DAAC at the National Snow and Ice Data Center.

CERES_EBAF-Surface_Ed2.8 Data Quality Summary (2015). Retrieved from http://ceres.larc.nasa.gov/documents/DQ_summaries/CERES_EBAF-Surface_Ed2.8_DQS.pdf

Choi, Y. S., Kim, B. M., Hur, S. K., Kim, S. J., Kim, J. H., & Ho, C. H. (2014). Connecting early summer cloud-controlled sunlight and late summer sea ice in the Arctic. *Journal of Geophysical Research: Atmospheres*, *119*, 11,087–11,099. https://doi.org/10.1002/2014JD022013

Christensen, M. W., Behrangi, A., L'ecuyer, T. S., Wood, N. B., Lebsock, M. D., & Stephens, G. L. (2016). Arctic observation and reanalysis integrated system: A new data product for validation and climate study. *Bulletin of the American Meteorological Society*, *97*(6), 907–916. https://doi.org/10.1175/BAMS-D-14-00273.1

Comiso, J. C., Parkinson, C. L., Gersten, R., & Stock, L. (2008). Accelerated decline in the Arctic Sea ice cover. *Geophysical Research Letters*, *35*, L01703. https://doi.org/10.1029/2007GL031972

Cox, C. J., Uttal, T., Long, C. N., Shupe, M. D., Stone, R. S., & Starkweather, S. (2016). The role of springtime Arctic clouds in determining autumn sea ice extent. *Journal of Climate*, *29*(18), 6581–6596. https://doi.org/10.1175/JCLI-D-16-0136.1

Curry, J. A., Schramm, J. L., Rossow, W. B., & Randall, D. (1996). Overview of Arctic cloud and radiation characteristics. *Journal of Climate*, *9*(8), 1731–1764. https://doi.org/10.1175/1520-0442(1996)009<1731:OOACAR>2.0.CO;2

Ding, Q., Schweiger, A., L'Heureux, M., Battisti, D. S., Po-Chedley, S., Johnson, N. C., et al. (2017). Influence of high-latitude atmospheric circulation changes on summertime Arctic sea ice. *Nature Climate Change*, *7*(4), 289–295. https://doi.org/10.1038/nclimate3241

Dong, X., Xi, B., Crosby, K., Long, C. N., Stone, R., & Shupe, M. (2010). A 10-yr climatology of Arctic cloud fraction and radiative forcing at Barrow, Alaska. *Journal of Geophysical Research*, *115*, D12124. https://doi.org/10.1029/2009JD013489

Dong, X., Zib, B. J., Xi, B., Stanfield, R. E., Deng, Y., Zhang, X., et al. (2014). Critical mechanisms for the formation of extreme arctic sea-ice extent in the summers of 2007 and 1996. *Climate Dynamics*, *43*(1-2), 53–70. https://doi.org/10.1007/s00382-013-1920-8

Herman, G., & Goody, R. (1976). Formation and persistence of summertime Arctic stratus clouds. *Journal of the Atmospheric Sciences*, *33*(8), 1537–1553. https://doi.org/10.1175/1520-0469(1976)033<1537:FAPOSA>2.0.CO;2

Heymsfield, A. J., Matrosov, S., & Baum, B. (2003). Ice water path–optical depth relationships for cirrus and deep stratiform ice cloud layers. *Journal of Applied Meteorology*, *42*(10), 1369–1390. https://doi.org/10.1175/1520-0450(2003)042<1369:IWPDRF>2.0.CO;2

Holland, M. M., & Bitz, C. M. (2003). Polar amplification of climate change in coupled models. *Climate Dynamics*, *21*(3–4), 221–232. https://doi.org/10.1007/s00382-003-0332-6

Huang, Y., Dong, X., Xi, B., & Deng, Y. (2018). A survey of the atmospheric physical processes key to the onset of Arctic sea ice melt in spring. *Climate Dynamics*, 1–16.

Huang, Y., Dong, X., Xi, B., Dolinar, E. K., & Stanfield, R. E. (2017). The footprints of 16 year trends of Arctic springtime cloud and radiation properties on September sea ice retreat. *Journal of Geophysical Research: Atmospheres*, *122*, 2179–2193. https://doi.org/10.1002/2016JD026020

Huang, Y., Dong, X., Xi, B., Dolinar, E. K., Stanfield, R. E., & Qiu, S. (2017). Quantifying the uncertainties of reanalyzed Arctic cloud and radiation properties using satellite surface observations. *Journal of Climate*, *30*(19), 8007–8029. https://doi.org/10.1175/JCLI-D-16-0722.1

Hurrell, J. W., Holland, M. M., Gent, P. R., Ghan, S., Kay, J. E., Kushner, P. J., et al. (2013). The Community Earth System Model: A framework for collaborative research. *Bulletin of the American Meteorological Society*, *94*(9), 1339–1360. https://doi.org/10.1175/BAMS-D-12-00121.1

Kapsch, M. L., Graversen, R. G., & Tjernström, M. (2013). Springtime atmospheric energy transport and the control of Arctic summer sea-ice extent. *Nature Climate Change*, *3*(8), 744–748. https://doi.org/10.1038/nclimate1884

Kato, S., Loeb, N. G., Rose, F. G., Doelling, D. R., Rutan, D. A., Caldwell, T. E., et al. (2013). Surface irradiances consistent with CERES-derived top-of-atmosphere shortwave and longwave irradiances. *Journal of Climate*, *2719-2740*(2013), 26.

Kay, J. E., Deser, C., Phillips, A., Mai, A., Hannay, C., Strand, G., et al. (2015). The Community Earth System Model (CESM) large ensemble project: A community resource for studying climate change in the presence of internal climate variability. *Bulletin of the American Meteorological Society*, *96*(8), 1333–1349. https://doi.org/10.1175/BAMS-D-13-00255.1

Kay, J. E., & Gettelman, A. (2009). Cloud influence on and response to seasonal Arctic sea ice loss. *Journal of Geophysical Research*, *114*, D18204. https://doi.org/10.1029/2009JD011773

Kay, J. E., Hillman, B. R., Klein, S. A., Zhang, Y., Medeiros, B., Pincus, R., et al. (2012). Exposing global cloud biases in the Community Atmosphere Model (CAM) using satellite observations and their corresponding instrument simulators. *Journal of Climate*, *25*(15), 5190–5207. https://doi.org/10.1175/JCLI-D-11-00469.1

Kay, J. E., L'Ecuyer, T., Chepfer, H., Loeb, N., Morrison, A., & Cesana, G. (2016). Recent advances in Arctic cloud and climate research. *Current Climate Change Reports*, *2*(4), 159–169. https://doi.org/10.1007/s40641-016-0051-9

Markus, T., Stroeve, J. C., & Miller, J. (2009). Recent changes in Arctic sea ice melt onset, freezeup, and melt season length. *Journal of Geophysical Research*, *114*, C12024. https://doi.org/10.1029/2009JC005436

McIlhattan, E. A., L'Ecuyer, T. S., & Miller, N. B. (2017). Observational evidence linking arctic supercooled liquid cloud biases in CESM to snowfall processes. *Journal of Climate*, *30*(12), 4477–4495. https://doi.org/10.1175/JCLI-D-16-0666.1

Minnis, P., Sun-Mack, S., Chen, Y., Khaiyer, M. M., Yi, Y., Ayers, J. K., et al. (2011). CERES edition-2 cloud property retrievals using TRMM VIRS and Terra and Aqua MODIS data—Part II: Examples of average results and comparisons with other data. *IEEE Transactions on Geoscience and Remote Sensing*, *49*(11), 4401–4430. https://doi.org/10.1109/TGRS.2011.2144602

Minnis, P., Sun-Mack, S., Young, D. F., Heck, P. W., Garber, D. P., Chen, Y., et al. (2011). CERES edition-2 cloud property retrievals using TRMM VIRS and Terra and Aqua MODIS data—Part I: Algorithms. *IEEE Transactions on Geoscience and Remote Sensing*, *49*(11), 4374–4400. https://doi.org/10.1109/TGRS.2011.2144601

Morrison, A. L., Kay, J. E., Chepfer, H., Guzman, R., & Yettella, V. (2018). Isolating the liquid cloud response to recent Arctic sea ice variability using spaceborne lidar observations. *Journal of Geophysical Research: Atmospheres*, *123*, 473–490. https://doi.org/10.1002/2017JD027248

Morrison, A. L., Kay, J. E., Frey, W. R., Chepfer, H., & Guzman, R. (2019). Cloud response to Arctic Sea ice loss and implications for future feedback in the CESM1 climate model. *Journal of Geophysical Research: Atmospheres*, *124*, 1003–1020. https://doi.org/10.1029/2018JD029142

Notz, D., & Stroeve, J. C. (2018). The trajectory towards a seasonally ice-free Arctic Ocean. *Current Climate Change Reports*, *4*(4), 407–416. https://doi.org/10.1007/s40641-018-0113-2

Serreze, M. C., Barrett, A. P., Stroeve, J. C., Kindig, D. N., & Holland, M. M. (2009). The emergence of surface-based Arctic amplification. *The Cryosphere*, *3*(1), 11–19. https://doi.org/10.5194/tc-3-11-2009

Serreze, M. C., & Stroeve, J. C. (2015). Arctic sea ice trends, variability and implications for seasonal ice forecasting. *Philosophical Transactions of the Royal Society A*, *373*(2045). https://doi.org/10.1098/rsta.2014.0159

Shupe, M. D., & Intrieri, J. M. (2004). Cloud radiative forcing of the Arctic surface: The influence of cloud properties, surface albedo, and solar zenith angle. *Journal of Climate*, *17*(3), 616–628. https://doi.org/10.1175/1520-0442(2004)017<0616:CRFOTA>2.0.CO;2

Taylor, P. C., Kato, S., Xu, K. M., & Cai, M. (2015). Covariance between Arctic sea ice and clouds within atmospheric state regimes at the satellite footprint level. *Journal of Geophysical Research: Atmospheres*, *120*, 12,656–12,678. https://doi.org/10.1002/2015JD023520

Wielicki, B. A., Barkstrom, B. R., Harrison, E. F., Lee, R. B. III, Smith, G. L., & Cooper, J. E. (1996). Clouds and the Earth's Radiant Energy System (CERES): An earth observing system experiment. *Bulletin of the American Meteorological Society*, *77*(5), 853–868. https://doi.org/10.1175/1520-0477(1996)077<0853:CATERE>2.0.CO;2